Microscale Capillary Wave Turbulence Excited by High Frequency Vibration

Jeremy Blamey,[†] Leslie Y. Yeo,[‡] and James R. Friend[*,¶,§]

Monash University, Clayton, Victoria 3168 Australia, MicroNanophysics Research Laboratory, RMIT University

Swanston Street, Melbourne, Victoria 3001 Australia, and MicroNanophysics Research Laboratory, SECE, RMIT University

Swanston Street, Melbourne, Victoria 3001 Australia

E-mail: james.friend@rmit.edu.au

Abstract

Low frequency (O(10 Hz–10 kHz)) vibration excitation of capillary waves has been extensively studied for nearly two centuries. Such waves appear at the excitation frequency or at rational multiples of the excitation frequency through nonlinear coupling due to the finite displacement of the wave, most often at one-half the excitation frequency in so-called *Faraday waves* and twice this frequency in superharmonic waves. Less understood, however, are the

[*]To whom correspondence should be addressed
[†]Monash University
[‡]RMIT University
[¶]RMIT University
[§]Melbourne Centre for Nanofabrication, 151 Wellington Road Clayton, Victoria 3168 Australia

dynamics of capillary waves driven by *high* frequency vibration ($> O(100\,\text{kHz})$) and small interface length scales, an arrangement ideal for a broad variety of applications, from nebulisers for pulmonary drug delivery to complex nanoparticle synthesis. In the few studies conducted to date, a marked departure from the predictions of classical Faraday wave theory has been shown, with the appearance of broadband capillary wave generation from 100 Hz to the excitation frequency and beyond, but there has not yet been a clear explanation. We show that weak wave turbulence is the dominant mechanism in the behavior of the system, evident from wave height frequency spectra that closely follows the Rayleigh-Jeans spectral response $\eta \sim \omega^{-17/12}$ as a consequence of a period-halving, weakly turbulent cascade that appears within a 1 mm water drop whether driven by thickness-mode or surface acoustic Rayleigh wave excitation. However, such a cascade is one-way, from low to high frequencies. The mechanism of exciting the cascade with high frequency acoustic waves is an acoustic streaming-driven turbulent jet in the fluid bulk, driving the fundamental capillary wave resonance through the well-known coupling between bulk flow and surface waves. Unlike capillary waves, turbulent acoustic streaming can exhibit subharmonic cascades from high to low frequencies; here it appears from the excitation frequency all the way to the fundamental modes of the capillary wave some four orders of magnitude in frequency less than the excitation frequency, enabling the capillary weakly turbulent wave cascade to form from the fundamental capillary wave upwards.

Introduction

Deceptively simple in appearance, capillary waves generated upon a fluid interface have provided nearly two centuries' worth of scientific interest, from the crispations of Faraday's era[1] to the development of entirely new analysis techniques in the modern era.[2] Ubiquitous in nature and man-made systems, from ocean waves to nebulisers, their importance in microfluidics comes as no surprise: capillary waves influence the bulk transport of drops and thin films driven by surface waves;[3–5] form cavitation at intense amplitudes and frequencies below a few MHz;[6,7] alter the

acoustic wave propagation within the fluid bulk;[8] affect micro-scale mixing,[9] particle concentration[10] and underlie atomisation, where the crests of large-magnitude capillary waves pinch off and are ejected to form a mist of fine droplets.[11–14]

The surprise is the appearance of relatively low-frequency capillary waves in these researchers' work, even when the frequencies of excitation ($> O(100\text{ kHz})$) are three or more orders of magnitude above the capillary waves' resonance frequencies ($O(10\text{ Hz})$–10 kHz). The two centuries of work on capillary wave phenomena have only considered the use of excitation at frequencies around or below the resonance frequencies of the capillary wave,[15,16] yet throughout the new literature where high frequency excitation is employed, capillary waves still appear and drive the consequent phenomena that are now widely used to creatively manipulate fluids. This remarkable discrepancy has only now started to be explored.[3,17,18] In the laboratory, capillary waves are traditionally generated by either directly perturbing the interface using a wavemaker,[15] a vibrating rod or plate penetrating the interface,[19] a microsphere in contact with the interface,[20] creative use of electric fields,[21] or—most typically—by parametrically inducing the waves through vertical vibration of the fluid container.[22–27]

A fluid surface excited by a perpendicularly-oscillating support may exhibit *Faraday waves* vibrating at one-half the excitation frequency,[1] in recognition of Faraday's discovery of these waves in a pool of mercury excited by hand in sunlight. Classical theoretical treatment of the Faraday problem gives, along the way, a Mathieu equation in terms of the interface displacement x_m,

$$\frac{d^2x_m}{dT^2} + (p_m - 2q_m\cos(2T))x_m = 0, \tag{1}$$

where $T = ft$, p_m is the ratio of the m^{th} discrete resonance ($m \in \{0,1,2,\ldots\}$) frequency f_m to the forcing frequency f, and q_m is proportional to the forcing amplitude.[28,29] The excitation of the surface comes from an explicit time-dependent coefficient in the equation of motion: the $\cos(2T)$ term adds energy to the system. Stability analysis shows that the response frequency of the Faraday

wave system depends on its representation in p–q space, defining the ratio of excitation frequency to natural frequency and the amplitude of excitation. Figure 2 of Benjamin and Ursell[28] shows the widely quoted $f/2$ response is only seen when the ratio p_m is of order one or less, and the amplitude of forcing is not greater than the order of the natural wavelength. A finite-amplitude analysis of the problem places greater restriction on the excitation frequency: that

$$\varepsilon \equiv (f - f_m)/f \ll 1, \tag{2}$$

for any resonance f_m;[29] in other words, the difference between the resonance frequency in question, f_m, and the excitation frequency, f, must be much less than the value of the excitation frequency itself.

This restriction in excitation frequency is overlooked, even omitted from a number of articles in the literature[15,30–32] leading to the erroneous application of Faraday wave theory when examining capillary waves in which the excitation frequency is many orders of magnitude greater than the fundamental natural frequency of the interface.[11,25,33,34] In this study, because we use extremely high excitation frequencies and therefore violate the condition presented by eq 2, Faraday wave theory as presented in the literature simply does not apply.

Furthermore, the fluid interface response cannot be fully described by a series of harmonic eigenmode resonances for finite-amplitude excitation; the response is inherently broadband in nature. The vibration response undergoes a transition from a discrete series of quantifiable, finite-amplitude eigenmode waves to a broadband continuum of waves at a very low amplitude of excitation.[12,35] The mechanism driving this change from discrete to continuous vibration spectra is the nonlinear, three-wave interaction between waves: after a set of travelling waves *collide*, the waves that arise from that interaction will extract some energy from the original set, but possess different energies, frequencies, and phases from each other and that original set. These new waves go on to interact with each other, the original set, and additional waves not a part of this original collision

to form other waves that likewise have new characteristics. And so on in a cascade of ever shorter wavelength waves with reduced amplitude.[36,37]

Such a broadband, power-law spectrum[12] is a strong indicator of turbulence-like nonlinear behaviour in a system.[22] Linear stability theory and similar approaches are therefore inappropriate under these circumstances, unfortunately, as they cannot accommodate the spatiotemporal exchanges in energy exhibited by these nonlinear systems. Kolmogorov[38] first proposed a Rayleigh-Jeans energy spectrum with respect to wavenumbers for isotropic hydrodynamic turbulence; the concept has since been applied to wave-like systems, where it has come to be known as *wave turbulence*.[37,39] Unlike the general case of hydrodynamic turbulence, wave turbulence is analytically tractable because the system can be simplified to a lower order,[37] an approach unavailable in an analysis of the vorticity in hydrodynamic turbulence. Kolmogorov-like wave turbulence solutions may be found for a great variety of systems, but the nature of the solutions and the route to finding them rely upon the Hamiltonian of the system;[40] the lowest-order non-zero nonlinear part of the frequency-domain Hamiltonian determines the number of waves which participate in the interactions. Capillary wave turbulence is a three-wave system; gravity wave turbulence, for example, is instead a four-wave system.

The theory of weak wave turbulence offers three important results pertinent to our capillary wave system: first, the power-law relation between the wave amplitude η and frequency f can be found[22,37] as $\eta \sim f^{-17/12}$ through dimensional analysis, as illustrated in the supporting information. The second important result is that the inertial range in time or length scale over which this power law applies exists between an energy source (so-called *pumping*) and an energy sink (fluid *damping*). As the cascade represents some transfer of energy from one length scale to another, a stationary solution which obeys the second law of thermodynamics requires an energy source and sink. Finally, it can be shown that the energy flux in wavenumber space must be positive. For capillary wave turbulence, this implies energy flows in one direction and *only* one direction: from its source at wavenumber k_0 to higher wavenumbers k_m where energy is damped. This result is a

property of the medium and appears as a consequence of the $-17/12$ power law and the dispersion relation.[41] Other media support *inverse* cascades, where the pumping wavenumber is greater than the damping, notably Langmuir waves in plasma,[42] but not capillary waves on fluids. The power-law relation between wave amplitude and frequency is readily observed: typical experiments in capillary wave turbulence employ a wave generator inside a large tank[19,43] or piston-like support excitation;[35] however, typical excitation frequencies are less than 10 Hz while the capillary wave phenomena appears at frequencies above this value.

Strong nonlinearities in a capillary wave system can give rise to rather more complex phenomena with a deviation from weak wave turbulence theory and the consequent power-law scaling. Lee *et al.*[40] found only recently that a renormalization of the dynamics and therefore the dispersion relationship enables determination of the wave spectra even with strongly nonlinear interactions. They note that a major question with weak wave turbulence theory remains with regard to what happens to real wave systems if any of the assumptions required in weak wave turbulence theory are violated. A platform permitting broad examination of the capillary wave phenomena, like the one described in this study, would be useful for this purpose.

In this work, we examine the peculiar behaviour of capillary waves in a microfluidic system as excited by high frequency acoustic waves between 500 kHz and 20 MHz. As our reference systems, we will consider the parametric vibration induced by both a thickness-mode lead zirconate titanate (PZT) transducer and a lithium niobate ($LiNbO_3$ or LN) based surface acoustic wave (SAW) device. These two devices provide different vibration motions and two exclusively different ranges of vibration frequencies—the former 1 to 1000 kHz and the latter 1 to 1000 GHz—and are representative of an entire class of devices finding application with some excitement in micro to nanofluidics.[17] Comparison with wave turbulence theory will show that turbulent capillary waves may be generated by extremely high-frequency excitation, far beyond what is typically reported in the literature, offering a new route to generating and studying these wave phenomena. Further, we explain the underlying phenomena driving the formation of the capillary waves and

their characteristics.

Generating and Measuring Microscale Capillary Waves

In order to measure the vibration of a capillary interface, we require a working fluid, an actuation device, and a means of measurement. For the fluid, a 2 $\mu\ell$ sessile hemispherical drop of deionised water was placed upon on a solid substrate set to vibrate to generate capillary waves upon the fluid interface as described later. A precision pipette (Eppendorf single channel adjustable 0.1–2.5 $\mu\ell$ pipette, North Ryde NSW Australia), mounted on a translation stage, was used to deliver the drop; in between experiments a regular protocol of cleaning using acetone, ethanol, deionized water, and dry nitrogen gas was used to clean the surface. These practices allowed us to avoid variations in drop size and contact angle from experiment to experiment; the contact angle was verified using a video microscopy system (Infinity K2/SC, Infinity Photo-Optical Company, Boulder, Colorado) with lab written contact angle measurement software in MATLAB (Mathworks, Chatswood NSW Australia). The drop size was allowed to vary as a parameter, although its volume was chosen to be less than the volume at which its shape significantly deforms due to gravity,[44,45] with a size less than the capillary length for gravity waves, $\ell = \sqrt{\gamma/(\rho g)} \approx 3$ mm for water, where γ is the surface tension and g is the acceleration due to gravity.[36] In the absence of gravity, the most relevant fluid property for capillary wave generation is the ratio of surface tension to density, fairly constant to an order of magnitude among most simple fluids, making the choice of working fluid somewhat arbitrary.

Two excitation devices were employed: PZT thickness-mode and LN SAW vibration devices. Both devices provide parametric excitation through the substrate but have distinctly different operating frequency ranges and motions; the former as an analog to published approaches and without vibration phase changes across the drop, albeit at a higher frequency of 500 kHz, and the latter as a specific method to examine very high frequency excitation at 20 MHz, though with an unusual

excitation motion that possesses rapid spatiotemporal phase changes across the drop. The pair was chosen to assess the effects of the method of excitation on the form of generated capillary waves; the SAW devices in particular are foreseen to be useful in a broad range of micro and nanofluidics devices that employ fluid interfaces,[17] but we will show the capillary wave phenomena they impart is also present in the simpler PZT thickness-mode system.

The PZT transducer, illustrated in Fig 1(a), possesses a thickness-mode resonance with a wavelength much larger than the contact area of the drop, akin to excitation motions typical in the literature.[23,24,26,30,36,46,47] Thickness-mode PZT transducers can be fabricated to effectively generate motion from a few kiloHertz to a few megaHertz. The thickness-polarized, face-electroded device used for this work (C–203, Fuji Ceramics, Tokyo, Japan; with Cr–Ag electrodes and dimensions as shown) was driven at its fundamental thickness-mode resonance at 500 kHz±2%; the variation is due to ambient temperature changes. While the amplitude of piston vibration is not uniform throughout such a disc, it was nearly uniform over the area of the drop's footprint. Because the surface of the Cr–Ag electrodes possesses micrometer-scale roughness, a sessile water drop will consistently form a contact angle of about 90°.

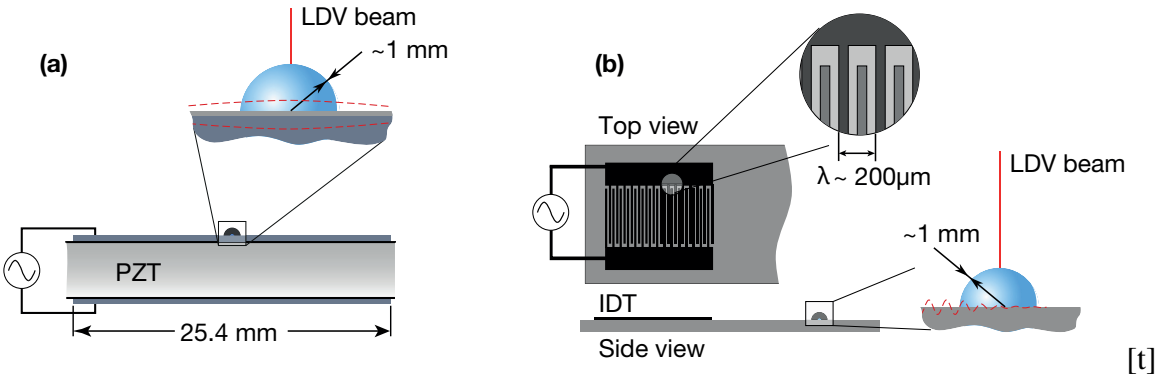

[t]

Figure 1: Schematic representation of (a) thickness-mode PZT and (b) SAW device actuation. For PZT, AC power is applied to electrodes on the upper and lower surfaces (upper surface shown in inset), inducing a thickness-polarized vibration mode at 500 kHz as indicated by the dashed line. The length scale of this deflection is greater than the contact length scale of the drop, $O(1\text{ mm})$, and so the phase under the drop is constant. For SAW, the Rayleigh wave is generated on the piezoelectric LN substrate at 19.425 MHz; the wave is damped as energy is absorbed by the fluid (schematically depicted in the inset with the dashed line).

The SAW device, illustrated in Fig 1(b), generates 19.425 MHz Rayleigh waves upon its surface due to the application of a sinusoidal electric signal to an interdigital transducer (IDT) patterned using photolithography on a single-crystal, piezoelectric, single-side polished, 127.68° Y-axis rotated cut, X-axis wave propagating LN substrate. The frequency was selected with precision through the definition of the simple IDT to resonate at a wavelength of 206 μm: in the simple IDT used here, the fingers and gaps between them all have a width of one-fourth the desired wavelength. In contrast to the PZT device, the SAW is a planar travelling wave and exhibits almost no resonance frequency variation, and generally operates at a much higher frequency between about 10–1000 MHz. The motion of the surface is elliptical and retrograde. Wave energy may be absorbed into a fluid in contact with the substrate through the phenomenon of "leaky SAW".[48] The principal features of SAW excitation are its high frequency, the fact the substrate has a rapid phase change in its displacement over the propagation path of the SAW, and the presence of in-plane and transverse components of vibration that are one-quarter of a wavelength in time out of phase with each other.

While SAW provides parametric excitation to a fluid in a manner similar to that described by Miles,[29] it fundamentally differs in that the SAW is a travelling Rayleigh wave with a wavelength so short that the phase of the wave spatially changes underneath the drop. Unlike the traditional wave-maker technique[19] and its variants,[20] under SAW excitation the fluid surface is never directly contacted by any apparatus except at the boundary. This makes SAW far more suitable for microscale devices: directly contacting the drop surface in any location would disturb the dynamics of the surface and possibly the internal fluid flow. SAW devices are capable of extremely narrow-band excitation (bandwidth is typically $< 0.005\%$ of the excitation frequency) over a range of frequencies from 1 MHz to 10 GHz, spanning four orders of magnitude. The particle velocity at the substrate surface as the SAW passes is typically $O(1$ m/s$)$, while displacements scale inversely with the SAW frequency and are generally $O(1$–100 nm$)$; acceleration scales with frequency and can be exceptionally large, up to $O(10^7$ m/s$^2)$. If the substrate is rigorously cleaned before use,

the surface is hydrophilic; however, the contact angle was consistently 90° using our procedure of cleaning and droplet deposition.

The excitation level is characterised here by measuring the transverse component of the vibration amplitude of the substrate. Electrical power input is sometimes selected as a basis for defining the behavior of the capillary waves; it is not appropriate here because the relationship between input power and vibration amplitude is very nonlinear, being dependent upon the electrical properties and the electro-mechanical coupling of the specific device, the temperature, and how these devices are mounted and driven. Our surface accelerations are typically between 15×10^6 to 90×10^6 m/s^2 for both devices, corresponding to 1–6 nm SAW amplitudes. Beyond 6 nm, the sessile drop tends to be transported across the substrate surface, and so measurement of the capillary wave is no longer reliable. Potentially the drop could be restrained with a well, but this may introduce a different boundary condition and additional complications in its excitation and was not considered here. Regardless, the electrical power used to drive drop vibration is generally less than 1 W.[12]

A laser Doppler vibrometer (LDV) (MSA-400, Polytec, Waldbronn, Germany) was used to measure the vibration velocity spectrum of the fluid surface[49] along the axis of the laser's path at its intersection with the measurement surface; the diameter of the measured area is approximately 1 μm.[49] This technique has several advantages over alternatives: high sensitivity (to $O(1\text{ pm})$); broad measurement range of DC to 25 MHz, where direct imaging or measurement of scatter through the surface[35] would require extremely high camera frame rates and correspondingly high-intensity illumination; and non-contact measurement, where other techniques in use require intrusive capacitive probes[19] that would distort the geometry of the drop. But the LDV has some drawbacks worth noting. First, the LDV directly measures vibration particle velocity along the laser path; this means the fluid surface must be nearly perpendicular to the incident beam, restricting the area of the drop we can measure to the central part to avoid substantial error in measurement.[50] Second, the signal returned by the vibrometer will contain information from all the laser energy to enter the detector; this includes not only the desired portion which has reflected from the

fluid surface, but also any light which has passed through the drop and reflected off the substrate. Shrinking the depth of field eliminates this issue; the fluid may also be coloured to absorb any light passing through the surface, although the colouring agent will change the properties of the fluid and lower the intensity of reflected light. In practice, the first effect has minimal impact if the measurement point is carefully positioned; coloured fluid experiments demonstrate the second effect affects only the magnitude of the measurement at the excitation frequency. Third, the limit of 25 MHz in measurement limits our ability to explore SAW excitation to the very lower end of such devices, precluding examination of higher frequency devices widely available to 1 GHz and beyond. Finally, the LDV is incapable of simultaneously measuring multiple points along the interface: it must *scan* from point to point making the measurement at each point one after another. Fortunately, as turbulent capillary waves may be considered a nearly ergodic system,[41] temporal and spatial ensemble averaging are considered equivalent. In order to observe stochastic properties of the system vibration, we must perform some manner of averaging on the spectrum. For this study, we ensemble average 360 spectra recorded sequentially in time at a single point, and benefit from the near-ergodicity of the system in the interpretation of the results.

Validation of Capillary Wave Weak Turbulence Theory

For deep-water capillary wave turbulence theory to apply to such a system, a number of assumptions must be validated: that the depth of fluid is much greater than the amplitude of the waves, that gravitational forces may be neglected, that the dispersion relation approaches

$$\omega^2 = (2\pi f)^2 = \frac{\gamma}{\rho} k^3, \tag{3}$$

and that the domain of the wave system be effectively infinite.

The linearised dispersion relation for deep-water capillary-gravity waves is widely accepted to

be

$$(2\pi f)^2 = gk + \frac{\gamma}{\rho}k^3; \tag{4}$$

for a flat interface. This implies a crossover frequency f^* from $(2\pi f^*)^2 = 2gk = 2\frac{\gamma}{\rho}k^3$ where gravity and capillary forces have equal importance; for water this crossover frequency is approximately 10 Hz. At frequencies greater than this, capillary forces dominate and the capillary wave dispersion relation reduces to eq 3.

Equations 3 and 4 are given in the context of an infinite flat interface. However, we show in the supporting information that, subject to interrelated constraints on wavenumber and wave amplitude, the relation for a curved surface typical of drops in our system is identical: for wave amplitudes of $O(10^{-9}$ m), eq 3 holds for frequencies $f \ll O(10^7$ Hz). We expect the linearised Lagrangian L of the system to take the form $L = a^2 G(k, f)$; by minimizing the variation of the Lagrangian we find $G(k, f) = 0$, giving the dispersion relation. Since the constant component of surface curvature does not participate in the variation, it will have no effect on G, and therefore does not alter the dispersion relation.

The assumption of infinite depth, on the other hand, requires that the product of wavenumber k and depth below the resting surface position h, $kh \gg 1$. Neglecting gravity, we assume h is of the same order as the radius of the drop, $O(1$ mm$)$ in our system; through the dispersion relation, the frequency associated with the limiting wave number is approximately 40 Hz.

The deep-water capillary wave dispersion equation can therefore be applied to a drop of radius $O(1$ mm$)$ over the frequency range 40 Hz $\ll f \ll 10^7$ Hz; we will show that all observed wave turbulent phenomena in our system occurs in this range.

As a final criterion for the applicability of wave turbulence theory, we must consider the effect of the pinned contact line and the finite domain. Wave turbulence theory assumes an infinite unbounded surface; however, such a domain is impractical for both numerical and experimental investigations. It has been shown that boundary effects do not dominate the response at all length

scales when the system is in a disordered state.[35] However, so-called "frozen turbulence", where wave energy is concentrated at resonant points in the spectrum, may occur where the length scale of the boundary is close to the length scale of interest,[51] although it is possible for "frozen" turbulence to exist side-by-side with broadband turbulence.[52] Fortunately, in our system the length scale of the boundary, $O(1\text{ mm})$, is larger than the capillary wavelength at frequencies beyond 1 kHz. Further, we are measuring the deflection at the center of the drop, the point farthest from the boundary possible. We expect that, as in past work,[35,51,52] the domain may be considered effectively infinite for the capillary waves we are examining.

Results

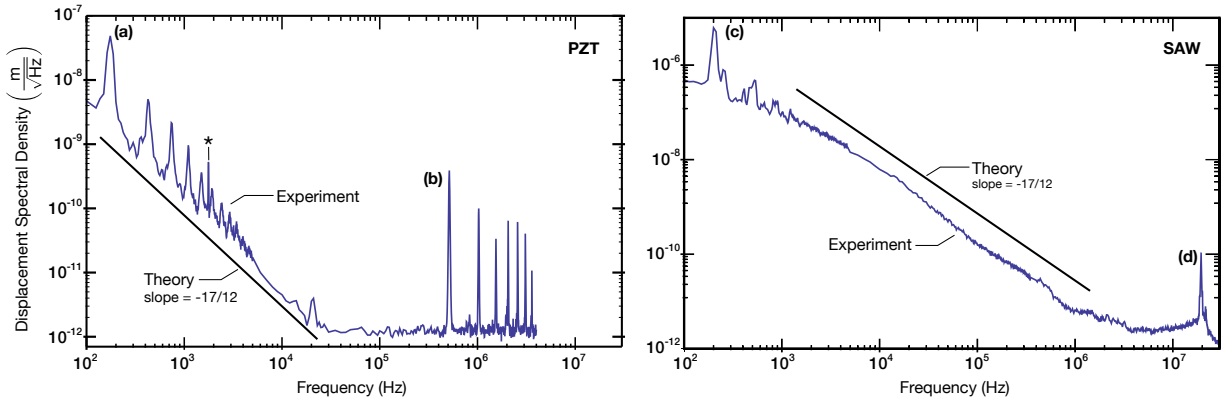

Figure 2: Typical vibration spectra for 500 kHz thickness-mode excitation via PZT (left) and 20 MHz Rayleigh wave excitation via SAW (right). Over the frequency range 100 Hz–2 kHz for the PZT and 1 kHz–2 MHz for the SAW, the experimentally measured spectra possess slopes that are remarkably close to $-17/12$, the value predicted by wave turbulence theory and indicated by the adjacent line. For PZT excitation, the (a) fundamental vibration mode is the largest response of the capillary wave, though successive resonances may be seen. The response decays to below the noise floor of the LDV at about 20 kHz, about 2 pm$/\sqrt{\text{Hz}}$, until the (b) Lorentzian response is seen about the excitation frequency of 500 kHz. Note the absence of subharmonic resonances but presence of superharmonic resonances at $2f$, $3f$,..., $7f$; for the SAW device, the superharmonics, if present, lie beyond the upper measurement limit of the LDV, 25 MHz. The (c) fundamental mode exhibits the largest response of the system to (d) SAW excitation at (b) 20 MHz, and the response at the excitation frequency is a Lorentzian distribution.

The LDV provides displacement spectral density distributions with respect to frequency from 100 Hz to 25 MHz, as illustrated in typical response spectra provided in Fig 2 for both the thickness-mode PZT device and the Rayleigh-wave generating SAW device. As previously observed,[8,12,49] note the presence of a capillary wave at the excitation frequency, remarkable given the very high frequency of the excitation in either case. This cannot be the response of the substrate because the focal depth is only sufficient to measure the fluid interface, the amplitude of vibration of the substrate is far lower than what is measured here, and the width of the response peak at the excitation frequency is far more narrow for the substrate: the response of the substrate absent the drop is identical to the noise floor except for a narrow peak at 500 kHz for the PZT and 20 MHz for the SAW device to a displacement spectral density amplitude of order 10^{-11} m/$\sqrt{\text{Hz}}$. As remarkable is the absence of a capillary wave at one-half the excitation frequency: there is no Faraday wave. Finally, note the presence of the capillary wave response at (Hz to kHz order) frequencies far lower than the excitation frequency.

The capillary waves do appear to behave as a system driven by weak wave turbulence. The majority of the spectra is dominated by a response cascade that follows a power-law relationship $\eta \sim f^{-1.420}$, closely correlated to the capillary wave turbulence theory-derived $-17/12 \approx -1.417$ slope ($R^2 = 0.990$ and 0.998 for the PZT and SAW devices, respectively), providing strong evidence of capillary weak wave turbulence in the system for two rather entirely different modes of fluid interface excitation.

The progression of resonant responses from the fundamental resonance frequency at about 200 Hz upwards appears according to the well-known[3,18,45] Lamb model of elastic resonance of a spherical capillary surface,[53]

$$f_m = \sqrt{\frac{(m+1)(m+2)(m+4)\gamma}{3\pi\rho L^3}} \tag{5}$$

providing the frequencies $f_m = \{247, 479, 742, 1030, 1350, 1700, \ldots\}$ Hz that correlate well with

the experimentally measured fundamental and higher-order resonances driven by the PZT device, $f_m = \{176, 432, 735, 1140, 1470, 1940, \ldots\}$ Hz ($R^2 = 0.999$), and the SAW device, $f_m = \{259, 506, 668, 862, 1220, 1688, \ldots\}$ Hz ($R^2 = 0.990$): there appears to be no need to resort to more thorough analysis provided elsewhere.[54] Note that there is nothing in these calculations that involve the excitation frequency. Further, there is a strong correlation ($R^2 = 0.961$) between the experimentally and theoretically determined fundamental resonance frequencies as the drop size is varied with the SAW device as illustrated in Fig 3. The exceptionally narrow peak indicated

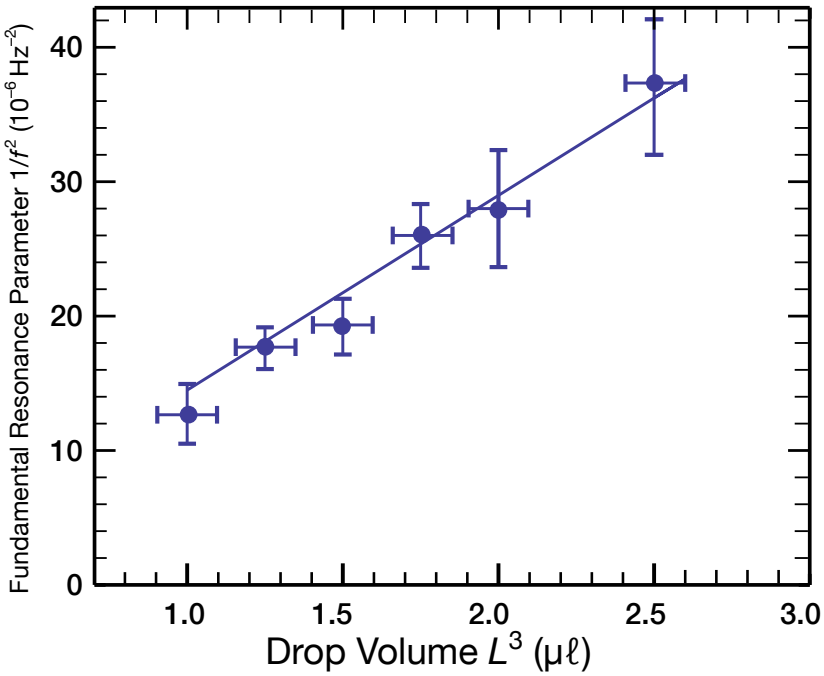

Figure 3: Driven by SAW at 20 MHz, the fundamental resonance frequency of the drop scales with the cube of its length according to eq 5 with good correlation ($R^2 = 0.961$); the line through the data represents the theoretical prediction. The error bars are twice the standard error; the horizontal error is due to pipetting as there was no observable evaporation effects for the short duration of each experiment. The data taken at each drop volume appear to be normally distributed ($n = 5$).

with an asterisk in Fig 2 is a specious single data point appearing due to the encoder card's analog-to-digital conversion at $2^{14} = 16,384$ Hz; its absence in the SAW-driven response is simply due to the stronger response driven by this system that acts to hide it under those conditions. Notably, there are no subharmonic cascades in this system from the excitation frequency at 500 kHz.

These results, taken altogether indicate that the system does not exhibit Faraday waves,[31] but more importantly, that it is behaving as a weak wave turbulent system.

For PZT excitation there are superharmonic resonances from the excitation frequency of 500 kHz upwards in a rational cascade $\{f, 2f, 3f, \ldots, 7f\}$, and perhaps beyond if not for encountering the upper limit of the LDV's measurement range at this resolution. The upper limit of the LDV's measurement range prevents us from determining whether there are similar superharmonic resonances in the SAW driven system.

The ultimate source of energy in this system is the parametric excitation, either from the SAW or PZT device; indeed the excitation frequency is strongly indicated by Lorentzian distributed drop surface vibration responses (*see* Fig 2(b,d); Lorentzian response distributions are characteristic of a second-order linear system with viscous damping). However, the strongest response whatever the excitation method appears at the drop's fundamental resonance frequency (*see* Fig 2(a,c)). The drop visibly vibrates in either case at its fundamental resonance under most conditions. The Faraday wave mechanism is clearly *not* the cause: the excitation of the fundamental drop resonance represents a downshift from the excitation frequency of three orders of magnitude for the PZT device and five orders of magnitude for the SAW device, far beyond the usual $f/2$ treatment resulting from the standard Mathieu equation-based result of Faraday wave analysis. Further, the capillary wave resonance frequencies clearly do not depend on the frequency of excitation, at odds with Faraday wave theory, not surprising given the violation of a fundamental precept of the theory in eq 2. However, the capillary wave resonances that appear at 200 Hz in Fig 2 *are* a consequence the physics of the capillary surface itself, as made clear by Fig 3.

We have shown here that the capillary waves behave under weak wave turbulence theory: their amplitude exhibits a Rayleigh-Jeans distribution of $\eta \sim f^{-17/12}$ over a broad frequency range. We will show now that this is actually a cascade from the fundamental capillary wave resonance frequency *upwards* in a one-way response. It is tempting to assume energy is transported from the high-frequency excitation to eventually give rise to the fundamental resonance of the drop through

a subharmonic cascade (akin to Lauterborn and Cramer[55]). However, the direction of energy flux for capillary wave weak turbulent spectra is *always* to greater frequencies: for capillary waves the energy source for the cascade *must be at a lower frequency* than the cascade itself, as discussed above.

The wave-turbulent cascade in our system is therefore *not* the mechanism by which the absorbed acoustic energy is shifted in frequency to the fundamental resonance: it cannot be for the excitation frequency is far higher than the entire capillary wave cascade. In fact, the cascade forms as a consequence of vibration at the fundamental resonance. It is apparent that the mechanism responsible for the downshift does not interfere with the capillary wave response at frequencies between the excitation and the fundamental mode, as the surface exhibits the theoretical stochastic wave-turbulent response.

So the question turns from why the response appears as it does to why it is excited in the first place. Turning now to focus upon the use of SAW excitation alone, we show that a mechanism permitting a *subharmonic* cascade from the high excitation frequency to the low capillary wave frequencies is the formation of turbulence in the acoustic streaming induced by the SAW within the fluid bulk.

Examining first the *streaming Reynolds number*[17] as a consequence of SAW excitation of the water drop,

$$\mathrm{Re}_{\mathrm{st}} = \frac{\rho \hat{u} L}{\mu} = \frac{\rho \left(u_{\mathrm{hyd}} + u_{\mathrm{vib}}\right) L}{\mu} = \frac{\rho \left[u_{\mathrm{hyd}} + (2\pi f x_{\mathrm{vib}})\right] L}{\mu} \sim \frac{\left(10^{3}\right)\left[\left(10^{-1}\right) + \left(2\pi 10^{7} 10^{-9}\right)\right]\left(10^{-3}\right)}{\left(10^{-3}\right)} \sim 10^{3}, \tag{6}$$

where ρ, L, μ, and $\hat{u} \equiv u_{\mathrm{hyd}} + u_{\mathrm{vib}}$ are the fluid density, drop size, fluid dynamic viscosity and Lagrangian fluid velocity, respectively; the last term being defined as a summation of the hydrodynamic fluid velocity in the drop, as observed to be on the order of $u_{\mathrm{hyd}} \sim 0.1$ m/s, and the vibration particle velocity as the acoustic wave passes through the fluid, u_{vib}, being dependent upon the am-

plitude of the vibration of the substrate. The streaming Reynolds number for PZT excitation is similar, because the Lagrangian fluid velocity is the same though the excitation frequency is two orders of magnitude lower.

A *streaming* Reynolds number of $\mathrm{Re}_{\mathrm{st}} \sim 10^3$ is well above the critical values of $\sim 10^2$ reported in the literature (and nicely explained in the classic article by Thompson, *et al*[56]) predicting a transition to *subharmonic, period-doubling cascades of turbulent fluid flow*[55] that result in chaotic flow behaviour. It is important to distinguish these results from those typical of hydrodynamic Reynolds number where there appears a transition to turbulence, for example, at values of 10^5 in "typical" pipe flow.[57]

The acoustic streaming can be shown to have become turbulent via another route. Lighthill[58] shows quite eloquently how turbulent *Stuart streaming* appears—with convective acceleration becoming significant—at only a few *micro*watts at 1 MHz. Taking a very conservative estimate for our system, assuming turbulent Stuart streaming appears when the acoustic streaming power, P, is above a critical value $P_{\mathrm{crit}} = 1$ mW, the power of the acoustic beam propagating into the fluid drop is $Pc\rho u_{\mathrm{vib}}^2 = c\rho f^2 \eta^2$ where c is the speed of the acoustic wave in the fluid, resulting in $\eta_{\mathrm{crit}} = (1/f)\sqrt{P_{\mathrm{crit}}/(\rho c)} = 0.61$ nm by solving for η_{crit} and substituting in typical values for water. This shows that for our SAW system we have turbulent acoustic streaming in all cases, with the 0.74 nm amplitude case near the critical amplitude, assuming that the amplitude of the acoustic wave is of the same order as the amplitude of the SAW the drop is residing upon, an assumption we have found to be valid elsewhere.[59]

The matter of turbulent acoustic streaming is important because it is key to explaining how a very high frequency acoustic excitation can result in such low frequency acoustic capillary waves, especially when there is no known mechanism to drive a subharmonic cascade in the capillary waves themselves. Unlike the capillary wave phenomena, a large-scale subharmonic cascade *is* possible in a turbulent jet,[55,56,58] and this appears to underlie the driving of low-frequency capillary waves by the very high frequency boundary vibration. The SAW-driven generation of turbulent

acoustic streaming in improving mixing in drops with geometries similar to this study has been shown to appear over a wide range of viscosities and powers,,[9] indicating how the bulk of the entire drop becomes turbulent through the acoustic streaming.

Other potential mechanisms of subharmonic coupling including interactions in the viscous boundary layer, bubble formation and collapse or interactions in and around these bubbles, or some other instability mechanism—especially the Kelvin-Helmholtz instability.[60] All these are unlikely: the first would require all of the energy of the capillary wave cascade to be transmitted through a exceedingly small part of the fluid drop's volume, since the viscous boundary layer only has a thickness on the order of 10 nm. The second potential mechanism has a similar volume constraint in addition to the fact that it is known bubbles are not formed with SAW excitation,[12] as opposed to what happens at much lower frequencies of excitation.[6,7] Kelvin-Helmholtz instabilities appear only upon sufficient flow speed at the fluid interface; the critical flow speed for our system would be $u_{\text{crit}} = \sqrt{2\sqrt{\gamma g \rho}} = 7.2$ m/s where γ is the air-water surface tension, and g is the gravitational acceleration.[60] Even presuming that the critical flow speed did not apply here, perhaps due to the presence of the turbulence, suggests the wavelength of the least stable wave due to the acoustic streaming flow is over 10 cm, well beyond the scale of our drop, suggesting that this form of instability is not responsible for the capillary waves we see.

However, the observation that the bulk flow and capillary wave are coupled through shear is well-known in the literature, as found by Longuet-Higgins[61] and shown convincingly by Trinh and Wang;[62] though the typical treatment of the phenomenon is the generation of the bulk flow by the capillary waves, here we see evidence of the process occurring in reverse, in a manner still consistent with their studies. In the absence of any detailed analysis of the formation of capillary waves due to bulk flow, if we take the liberty of considering the classical solution of Stokes' drift[61] due to capillary waves, $u = \eta^2 \omega k \mathrm{e}^{-2kz}$ where z is the distance into the flow of the deep bulk (using a shallow treatment prevents solution here), and note that the Stokes' drift in this context is also the time-averaged fluid flow in the bulk u induced by the turbulent acoustic jet, we can determine

what order the velocity of the turbulent jet would have to be to induce the fundamental capillary waves we observe. With the relationship as written, $u \sim \eta^2 \omega k = \omega^{-11/6} k$ if we note the capillary weak wave turbulence relation $\eta \sim \omega^{-17/12}$. Since the fundamental vibration mode is at about 250 Hz and its wavelength is about 1 mm, consequently $u \sim 10$ mm/s. If instead we chose to note that the typical amplitude of the fundamental vibration mode is on the order of 100 μm, again $u \sim$ 10 mm/s. Either way, the turbulent acoustic jet is driving flow in the drop at these velocities and beyond, and the turbulence of the acoustic streaming is present to drive formation of the capillary wave at these frequencies, so via this simplistic treatment it appears entirely possible to drive capillary waves of the form we see with the acoustic streaming we know to be present in the drop. Certainly more appropriate and detailed analysis, properly incorporating the nonlinearities in lieu of reference to classic theory, would provide a more detailed picture of the mechanism responsible for the capillary waves.

We turn now to examine the dynamics of the drop through its vibration spectrum at different excitation levels. Figure 4(a) indicates the noise floor of the LDV, in other words, the minimum displacement spectral density as a function of frequency, a function of ambient noise, thermal noise, analog-to-digital conversion limitations, and the shot noise of the measurement system. These culminate in a constant velocity, $1/f$, noise over the range 10^4– 10^5 Hz due to the limitations of the analog-digital encoder hardware in the LDV, while beyond 10^5 Hz the noise floor is defined by a constant value of about $0.5\ /\sqrt{\text{Hz}}$ due to shot noise at the photodiode of the LDV. The asterisks refer to specific peaks present due to intrinsic encoder difficulties (as with all such encoders) at $2^{13}, 2^{14}, 2^{15}$ Hz that are not true resonance peaks. The noise floor coincidentally matches the theoretical slope from 300 to 2000 Hz but does not match elsewhere.

The capillary wave response transforms from a discrete to continuous response as the SAW amplitude is increased. Upon application of SAW to the drop at 20 MHz, the response at that same frequency appears as a narrow peak in Fig 4(b), which grows as the excitation amplitude is increased to 1.6 nm but remains relatively constant as the excitation amplitude is increased further

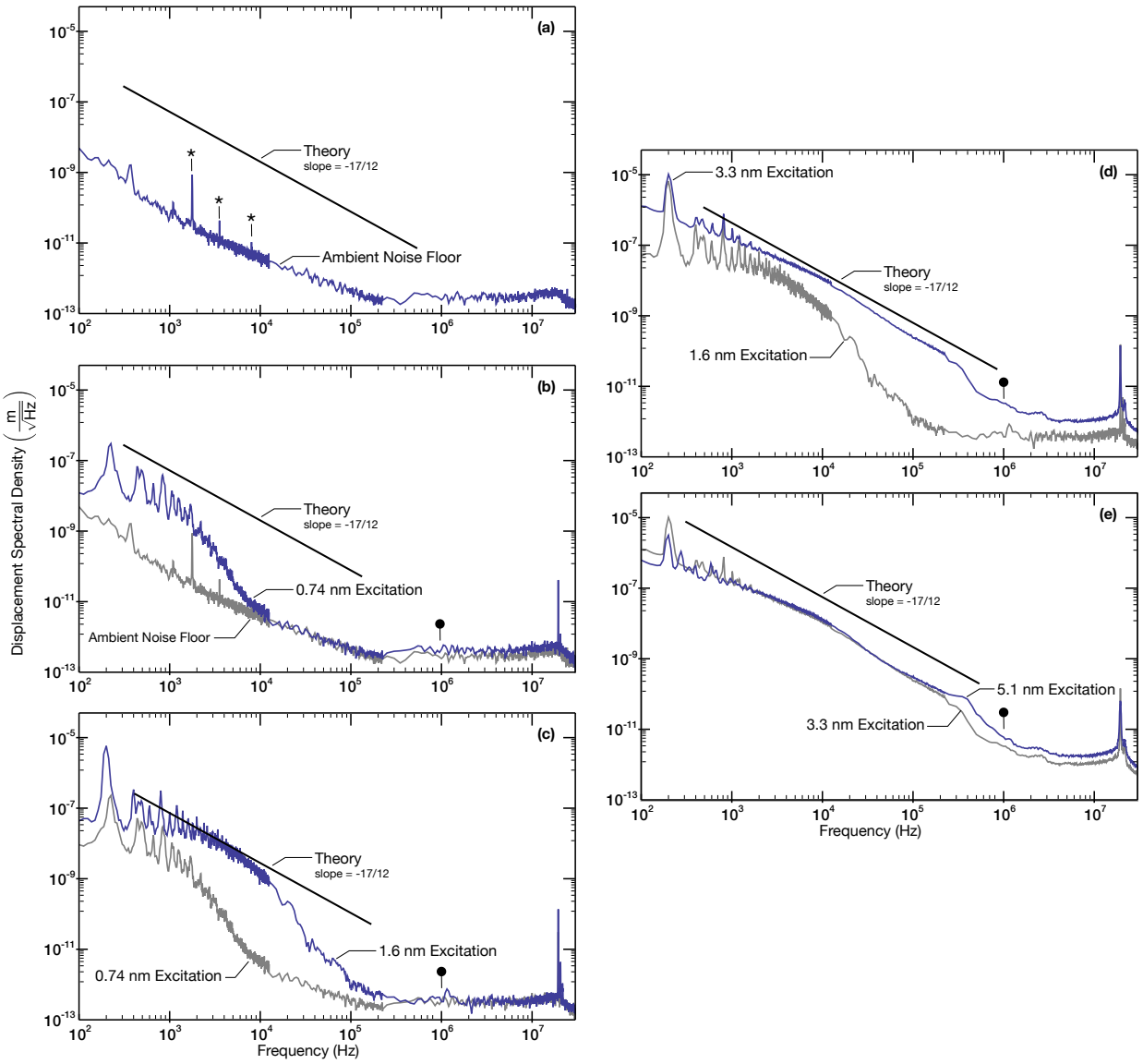

Figure 4: Evolution of the spectrum with increasing SAW excitation amplitude; (a) ambient noise floor without explicit vibration excitation, (b) 0.74 nm by comparison to ambient, (c) 1.6 nm excitation compared to 0.74 nm excitation, (d) 3.3 nm excitation compared to 1.6 nm, and (e) 5.1 nm versus 3.3 nm excitation.

to 5.1 nm: the energy is moving elsewhere in the spectrum. As the excitation level increases, the response of the drop at low frequencies begins to saturate (c); energy then enters the wave turbulent cascade (d). At high excitation level (e), the turbulent cascade is fully established over an inertial range spanning at least 10^3–10^6 Hz. Another indicator of the turbulent response is the smoothened broadband response at the highest excitation levels (d,e) from the discrete resonances that appear at relatively lower excitation amplitudes (b,c), except for the ever present and substantial fundamental resonance of the drop at around 200 Hz.

Figure 4(b–e) illustrates this by comparison of the displacement response due to a given level of excitation to the next lowest level of excitation; Fig 4(c), for example, shows the response to 1.6 nm excitation is very similar to the 0.74 nm response between 100 Hz and 1000 Hz, but is very different between 1000 Hz and 50 kHz. Low-frequency vibration appears at even the lowest excitation levels we could sustainably operate, 0.74 nm, and this response propagates upwards in frequency to fill in the turbulent cascade from 200 Hz to—eventually—1 MHz as the excitation is increased to 5.1 nm. The discrete response of the system and absence of a complete cascade at 0.74 nm indicates that we are likely on the lower bound of excitation of the turbulent acoustic streaming and consequently the formation of the capillary waves (predicted to occur at 0.61 nm above); future work could consider this transition in far more detail. Curiously, there is little difference between an excitation of 3.3 nm and 5.1 nm in Fig 4(e) other than the appearance of a "hump" in the higher amplitude response which appears to be correlated to the appearance of atomisation phenomena, an aspect for consideration in a separate work. It is important to remember the effect of operating with such high excitation frequencies with regard to the incredible accelerations imparted to the drop: though the displacements are only 0.74, 1.6, 3.3, and 5.1 nm, the respective accelerations are 11, 23, 50, and 76×10^6 m/s^2 for these four levels of excitation.

We should expect the inertial range to end with wave energy being rapidly damped beyond some threshold wavenumber, as shown in other studies.[43] In such a case, the cascade will steepen in descent away from the theoretical gradient.We see this behavior in Fig 4(b) from 10^3 to 10^4 Hz,

in Fig 4(c) over $10^4 \sim 10^5$ Hz, and $5 \times 10^5 \sim 10^6$ Hz in Fig 4(d). The presence of the noise floor of the LDV precludes our ability to measure this phenomena beyond about 1 MHz. The vibrometer's claimed displacement resolution at MHz-order frequencies is less than 0.1 pm$/\sqrt{\text{Hz}}$; our measurements show the spectrum becomes constant at a noise floor of $O(0.01$ pm$/\sqrt{\text{Hz}})$ at $O(10^7$ Hz$)$. An alternate perspective is provided by calculating the Kolmogorov viscous time scale in water, $\tau = \left(\frac{\nu}{\varepsilon}\right)^{1/2} \sim O(1$ MHz$)$; 1 MHz has been indicated with a solid circle on Figure 4(b–e), nominally representing the end of the capillary wave cascade, which appears consistent with the experimentally measured results.

The evolution of the low frequency resonance with increasing excitation level is also apparent in Fig 4. The harmonic series of low frequency resonances is quite typical of *narrow-band pumping*:[22,41] pumping energy is localised around a specific frequency or characteristic length, in contrast to *wide-band pumping* where the pumping is spread over a range of frequencies, an extreme example being the excitation of drops by white noise.[63] Here, the energy is initially concentrated at the frequency of pumping; interactions between two waves generated by the pumping lead to energy transfer to the next harmonic in the series, and similar processes lead to the creation of ever shorter and wider harmonic peaks that gradually merge with the background level of the spectrum at higher frequencies. All of the spectra, regardless of excitation amplitude, exhibit zero frequency side bands, exponential decay, and power law behaviour; phenomena that according to Xia and Punzmann[35] imply the presence of turbulence throughout. Turbulence is already present from low excitation levels; increasing the amplitude of excitation acts to distribute the power to higher frequencies.

The low-frequency interactions are governed by the same weakly nonlinear mechanics as the cascade at higher frequencies. However, the effects of eigenmode resonances of the drop surface and initial energy concentration at the fundamental vibration mode combine to limit the interactions between waves, constrained by the three-wave resonance conditions $f_1 = f_2 + f_3$ and $\mathbf{k}_1 = \mathbf{k}_2 + \mathbf{k}_3$, to a set of discrete harmonics. We observe the harmonic series, steadily decreasing

in magnitude with higher frequency, superimposed upon a broadband level decreasing at a slower rate than the harmonic peaks. This is evident in Fig 4(b,c); as the excitation amplitude increases beyond 1.6 nm the spacing between adjacent resonances become narrower in the frequency domain.

Conclusions

To conclude, we have described a method to parametrically generate and measure capillary wave phenomena at the micro-scale using laser Doppler vibrometry, MHz-order SAW actuation and kHz-order thickness-mode actuation, inducing fluid flows that exhibit strongly inertial behavior. Capillary waves appear at the frequency of excitation as a linear response to the excitation, but also—and most remarkably—appear at much lower frequencies, from the fundamental resonance frequency upwards as a discrete modal response at low excitation amplitudes that gives way to a continuous broadband response.

The turbulent Rayleigh-Jeans power-law cascade and pumping characteristics in our system behave as per weak wave turbulence theory, despite the fact the excitation frequency is substantially higher than the capillary wave response frequencies, regardless of whether the system is driven through thickness vibration or surface acoustic wave vibration, and despite the exceptionally large accelerations induced in the system. Notably, strongly nonlinear phenomena that might have renormalized the expected Zakharov-Kolmogorov turbulence spectrum,[40] was not seen, a surprise considering the extreme accelerations induced by the SAW. The key aspects of weak turbulence theory this system was observed to conform to include

1. The capillary wave amplitude $\eta \sim f^{-17/12}$, between the energy source frequency and the energy sink frequency.

2. The energy flux in wavenumber space must be positive: energy flows from a source at a low k_0 to a high k_m; $k_m > k_0$ is required and therefore the capillary wave energy must flow from

low frequencies to high frequencies.

Finally, no Faraday wave response was detected in this system, a consequence of the excitation frequency being far greater than the observed capillary wave frequencies, atypical in many experiments studying capillary wave phenomena but a feature of many new acoustically driven microscale devices under consideration.

Through the known one-way nature of capillary wave weak turbulence with its energy flow from low to high frequencies, we may infer that the fundamental capillary wave resonance appears to be directly driven by the parametric excitation at very high frequency, through acoustic streaming-driven chaotic flow in the fluid bulk. The acoustic streaming was found to be turbulent due to the presence of convective acceleration when the induced vibration amplitude for the SAW was greater than 0.61 nm, over the entire measurement range of this study. Though alternative routes of coupling to form capillary waves from the incident acoustic wave were considered, the most likely candidate remains the turbulent acoustic streaming inducing bulk flow within the drop that drives the generation of the capillary waves through shear. In any case, the turbulence in the jet *can* support energy flow from high excitation frequencies to the low frequencies of the capillary wave phenomena, and it is this mechanism that drives the subsequent formation of the low-to-high frequency capillary wave cascade.

Acknowledgement

This work was conducted at the Melbourne Centre for Nanofabrication (MCN) and was supported by Australian Research Council grants DP120100013, DP120100835, and NHMRC grants 1000513 and 546238. JRF is grateful to the Melbourne Centre for Nanofabrication for a Senior Tech Fellowship, and to RMIT University for a Vice-Chancellor's Senior Research Fellowship. LYY is grateful for an Australian Research Fellowship from the Australian Research Council under grant DP0985253.

Supporting Information Available

Capillary wave weak turbulence and the scaling of wave energy

Following the approach developed by Zakharov,[41] we define the occupation number $n(\mathbf{k},t)$, a function of the wave vector $\mathbf{k}$ and time, by the energy density $e = f(k)n(\mathbf{k},t)$; wave frequency is considered a function of the wave number through the dispersion relation in eq 3 for capillary waves. Continuity of energy can then be expressed as $\frac{\partial e}{\partial t} + \nabla \cdot p(\mathbf{k},t) = 0$; p is the energy flux in k space. Therefore,

$$\nabla \cdot p(\mathbf{k},t) = \omega(k) I(\mathbf{k},t), \tag{7}$$

where $I(\mathbf{k},t)$ is defined by the so-called stationary kinetic equation,[41]

$$\begin{aligned} \frac{\partial n}{\partial t} &\equiv I(\mathbf{k},t) \\ &= \pi \int |V_{k12}|^2 f_{k12} \\ \delta(\mathbf{k}-\mathbf{k}_1-\mathbf{k}_2)\delta(\omega-\omega_1-\omega_2) &+ (...) d\mathbf{k}_1 d\mathbf{k}_2; \end{aligned} \tag{8}$$

$k12$ represents a function of variables $\mathbf{k}, \mathbf{k}_1, \mathbf{k}_2$, f_{k12} scales as $n(\mathbf{k},t)^2$ and the terms represented by the ellipsis are defined by permutation in the k variables, substituting k_1 for k, k_2 for k_1, and so on. The form of V_{k12} is known, but for this discussion only its scaling with respect to k, $V(k) \sim V_0 k^m$, is significant: from dimensional analysis of the system Hamiltonian, $m = 9/4$. The two delta functions enforce 3-wave interactions.

If we assume a power-law scaling for n against k, $n(k) = Ak^{-s_0}$, then the scaling of I with respect to area in k space becomes

$$I(\mathbf{k},t) \sim (V_0^2 k^{2m})(A^2 k^{-2s_0})(k^d), \tag{9}$$

where the integrating variables have been collected under the k^d term; d represents the dimensionality of the problem; for surface waves, $d = 2$.

Taking the integral form of eq 7,

$$P(k) = -\pi \int_0^k \omega(k) I(\kappa) (2\kappa)^{d-1} d\kappa; \tag{10}$$

we note that the frequency does not depend on the integrating variable, due to the Dirac delta functions inside $I(k)$. Substituting the scaling from eq 9, we have

$$P(k) \sim \omega \int V_0^2 A^2 k^{2m+d-2s_0} k^{d-1} dk. \tag{11}$$

We require $P(k)$ to be constant with respect to k;[41] in that case $2m + 2d - 2s_0 = 0$; since m is known to be 9/4 and $d = 2$, the power-law relation for $n(k)$ is thus

$$n(k) = Ak^{-17/4}. \tag{12}$$

Through the dispersion relation, we can find an equivalent scaling for n against angular frequency,

$$n(\omega) = A'\omega^{-17/6}. \tag{13}$$

The occupation number n is not directly measurable. However, it can be directly related to the two-point correlation of surface deflection η, $\langle \eta(t)\eta(\tau + t)\rangle \sim n$,[37] and thus

$$\eta \sim \omega^{-17/12} \sim f^{-17/12}. \tag{14}$$

The power law scaling of occupation number,[37,41,64] energy and surface deflection[19,35] are confirmed in the literature.

Dispersion relation on a curved surface

There exists a class of wave motions termed dispersive, as distinct from (for example) hyperbolic waves. Linearising the wave equation for such waves will yield a relation

$$G(\omega, \mathbf{k}) = 0, \tag{15}$$

known as the dispersion relation; it relates the frequency ω of a linear wave to the wavelength $\lambda = 2\pi/k$. $\mathbf{k}$ is the wave vector; its magnitude is k, the wavenumber.

While it has been emphasised that the dispersion relation applies to a linear system, it is applied in various ways in the analysis of non-linear systems. In such systems the dispersion relation is still considered to relate a wavelength with its corresponding wave frequency.

For this derivation, we choose to use a calculus of variations method. Following Whitham,[65] we assume a wave train with wave height η of the form

$$\eta \sim a\cos(\alpha), \tag{16}$$

where $\alpha = \mathbf{k}\cdot\mathbf{x} - \omega t$ and the amplitude a, wave vector $\mathbf{k}$, and frequency ω are considered "slowly varying" (that is, their derivatives are neglected); the independent variables are position vector $\mathbf{x}$ and time t. The Lagrangian L is then constructed as

$$L = T - V \tag{17}$$

with kinetic energy T and potential energy V. It is understood[65] that for any linear problem, L must take the form

$$L = G(\omega, \mathbf{k})\, a^2, \tag{18}$$

and since the solution for non-zero variation δa requires

$$\frac{\partial L}{\partial a} = 0, \tag{19}$$

then

$$G(\omega, \mathbf{k}) = 0 \tag{20}$$

provides the dispersion relation.

We shall derive here the dispersion relation for the case of low-amplitude high-frequency linear waves. The resting curvature of the surface shall be considered uniform; that is, we are assuming a spherical domain. The geometry of interest is that of a surface whose resting shape is uniformly curved; that is, a spherical surface. For reference, however, we shall illustrate the solution technique first for an infinite flat surface, before deriving the solution for the curved surface.

Dispersion relation on a flat surface

This derivation is made for comparison only; the result may be verified in any text dealing with water waves. The subsequent derivation for a curved surface is of more interest, and we shall explore assumptions more carefully there.

We shall consider an infinite plane interface between a fluid of infinite depth and density ρ below, and a fluid of negligible density above. Such an arrangement models a deep water surface in an atmosphere of air. At rest, the interface occupies the x, y plane; that is, $z = 0$. The position vector $\mathbf{r}$ for any point on the surface is defined as

$$\mathbf{r} = x\hat{\mathbf{e}}_x + y\hat{\mathbf{e}}_y + \eta\,(x, y, t)\,\hat{\mathbf{e}}_z. \tag{21}$$

To construct the Lagrangian as per eq 17, we assume that wave height is of the form of eq 16;

the potential term is

$$V = V_g + V_\gamma \tag{22}$$

where V_g is the gravitational potential energy

$$\begin{aligned} V_g &= \iiint_0^\eta \rho g z \, dx\, dy\, dz \\ &= \frac{1}{2}\rho g \iint \eta^2 \, dx\, dy \end{aligned} \tag{23}$$

and V_γ is the potential energy due to surface tension

$$V_\gamma = \gamma \iint (dS - dA), \tag{24}$$

where γ is the interfacial surface tension; dS represents an infinitesimal element of surface area, while dA represents the uncurved area $dx\,dy$. Recognising that

$$dS = |\mathbf{r}_x \times \mathbf{r}_y| \, dx\, dy \tag{25}$$

(subscripts denote partial differentials), we find

$$dS = \sqrt{\eta_x^2 + \eta_y^2 + 1} \, dx dy, \tag{26}$$

and hence

$$V_\gamma = \gamma \iint \left(\sqrt{\eta_x^2 + \eta_y^2 + 1} - 1 \right) dx dy. \tag{27}$$

If we assume $\eta_x^2, \eta_y^2 \ll 1$, we may further simplify this to

$$V_\gamma = \frac{1}{2}\gamma \iint \left(\eta_x^2 + \eta_y^2 \right) dx dy. \tag{28}$$

Finally, the kinetic energy is found from the gradient of the flow potential ψ as

$$T = \frac{1}{2}\rho \iiint_{-\infty}^{\eta} |\nabla \psi|^2 \, dx\,dy\,dz. \tag{29}$$

Assuming η is small, we can replace the upper limit of integration $z = \eta$ by $z = 0$. Then, using Green's first identity and the assumption that the flow is irrotational, we have

$$T = \frac{1}{2}\rho \iint \psi \frac{\partial \psi}{\partial z} \, dx\,dy. \tag{30}$$

To obtain the dispersion relation, we simply have to substitute in the flow potential and surface height functions. For simplicity, let us consider a wave propagating in the x-direction; the argument α from eq 16 is then

$$\alpha = kx - \omega t. \tag{31}$$

The flow potential ψ satisfies both the Laplace equation

$$\nabla^2 \psi = 0 \tag{32}$$

and the velocity boundary condition at the surface,

$$\left.\frac{\partial \psi}{\partial z}\right|_{z=\eta} = \frac{\partial \eta}{\partial t} \tag{33}$$

$$= \omega a \sin(\alpha). \tag{34}$$

If we again approximate $z = \eta$ by $z = 0$, we may find, using separation of variables,

$$\psi(x,z,t) = \frac{1}{|k|} e^{|k|z} \omega a \sin(\alpha). \tag{35}$$

Thus the energies at the interface become

$$T = \frac{1}{2}\rho \iint \frac{\omega^2 a^2}{k} \sin^2(\alpha)\, dx\, dy, \tag{36}$$

$$V_g = \frac{1}{2}\rho g \iint a^2 \cos^2(\alpha)\, dx\, dy, \tag{37}$$

$$V_\gamma = \frac{1}{2}\gamma \iint k^2 a^2 \sin^2(\alpha)\, dx\, dy. \tag{38}$$

We then integrate over one period to find the phase-averaged Lagrangian

$$L = \frac{1}{4}\left[\rho\frac{\omega^2}{k} - \rho g - \gamma k^2\right] a^2 \tag{39}$$

and recalling eq 20 we can conclude that

$$\omega^2 = gk + \frac{\gamma}{\rho}k^3. \tag{40}$$

Derivation for dispersion on a spherical surface

For this derivation, we shall neglect the gravitational term. Equation 40 allows us to assume that gravitational effects are negligible for frequencies greater than $O(10^2$ Hz), or equivalently wavelengths shorter than $O(10^{-3}$ m). In fact, as we consider this problem in the context of a sessile drop of diameter $O(1$ mm), we shall assume that the wavelength must be substantially shorter than this, as it is obvious that wavelengths longer than the diameter of the sphere cannot be considered. As such, our omission of the effects of gravity is henceforth justified.

We shall consider the complete surface of the sphere. The position vector is simply

$$\mathbf{r} = r\hat{\mathbf{e}}_r, \tag{41}$$

$$r = r_0 + \eta, \tag{42}$$

while the angular coordinates are the aziumth θ and the latitude relative to the bisecting plane, ϕ. The sphere is of radius r_0. Rather than consider a travelling wave as per eq 16 we will assume, for reasons which will become clear, an axisymmetric standing wave surface deflection of

$$\eta = a\cos(kr_0\phi)\cos(\omega t). \tag{43}$$

We will construct the Lagrangian in a similar manner to the previous derivation, that is

$$L = T - V_\gamma \tag{44}$$

where V_γ is as per eq 24 and T is similar in form to eq 29:

$$T = \frac{1}{2}\rho \iiint_0^\eta |\nabla\psi|^2 r^2 \cos\phi \, dr \, d\theta \, d\phi. \tag{45}$$

To compute the local curvature, surface area and normal vectors of the surface due to the wave, we will use the non-dimensional surface height $r^* = r/r_0 = (r_0+\eta)/r_0 = 1+\eta^*$. The element of surface dS is then

$$\begin{aligned} dS &= r_0^2 (dS^*) \\ &= r_0^2 \left(\left| \mathbf{r}_\theta^* \times \mathbf{r}_\phi^* \right| r^{*2} \cos\phi \, d\theta \, d\phi \right) \\ &= r_0^2 \left((1+\eta^*) \sqrt{1 + \frac{\eta_\theta^{*2}}{(1+\eta^*)^2} + \frac{\eta_\phi^{*2}}{(1+\eta^*)^2}} \quad r^{*2} \cos\phi \, d\theta \, d\phi \right), \end{aligned} \tag{46}$$

where the subscripts refer to partial derivatives.

Here we make our first simplification, that

$$\eta^* \ll 1, \text{ and thus} \tag{47a}$$

$$r^* \approx 1. \tag{47b}$$

Measured spectral amplitudes of vibration are $O(1\text{ nm})$, and the radius r_0 is $O(10^{-3}\text{m})$, so typically $\eta^* \sim O(10^{-6})$. Considering the partial derivatives of surface height,

$$\eta^*_\phi = -kr_0 a^* \sin(kr_0\phi)\cos(\omega t) \tag{48}$$

$$\sim O(k)O(\eta), \tag{49}$$

remembering that $a^* \equiv a/r_0 \sim O(\eta)/O(r_0)$. Therefore, to consider $\eta^*_\phi \ll 1$, we require $k \ll O(\eta)$; if we assume for the moment that eq 40 holds, this implies that $\omega \ll O(10^7\text{ Hz})$. The assumption is therefore not unreasonable.

It should be noted at this point that the assumption $\eta^*_\phi \ll 1$ simplifies the application of Green's first identity for the kinetic energy equation (transforming eq 29 to eq 30), allowing us to replace the normal vector with the radial vector.

Returning to the element of area, applying the above assumptions yields

$$dS = r_0^2\left(\frac{\eta^{*2}_\phi}{2}\cos\phi\, d\theta\, d\phi\right), \tag{50}$$

which, substituted into eq 24 and including eq 48, gives

$$V_\gamma = \frac{1}{2}r_0^2\gamma\iint \eta^{*2}_\phi \cos\phi\, d\theta\, d\phi \tag{51}$$

$$= \frac{1}{2}r_0^2\gamma\iint k^2a^2\sin^2(kr_0\phi)\cos^2(\omega t)\cos\phi\, d\theta\, d\phi. \tag{52}$$

Turning now to the flow potential function, we impose boundary conditions analogous to those

of the previous analysis, eq 32 and

$$\left.\frac{\partial \psi}{\partial r}\right|_{r=r_0} = \frac{\partial \eta}{\partial t}. \tag{53}$$

Applying separation of variables,

$$\psi = R\Phi, \text{ where} \tag{54}$$

$$R = \sum_{l=0}^{\infty} A_l r^l \tag{55}$$

$$\Phi = P_l(\cos\phi), \tag{56}$$

where P_l is the l^{th} Legendre polynomial. Allowing l to become large, we approximate $P_l \approx c\cos l\phi$, where c is "slowly varying" relative to the argument of the cosine function; because the argument of the Legendre polynomial is $\cos\phi$, Φ is always an even function. Strictly speaking, the boundary condition disallows travelling wave solutions. This then is the reason why we have chosen to consider a standing wave (eq 43) rather than a travelling wave as before. Proceeding from eq 53 and eq 54,

$$\left.\frac{\partial \psi}{\partial r}\right|_{r=r_0} \equiv \left. R'\Phi\right|_{r=r_0} = -\omega a \sin(\omega t)\cos(kr_0\phi); \tag{57}$$

we set $l = kr_0$, and thus for R' (recalling eq 55, letting $A_l = 0$ for $l \neq kr_0$, and correcting a/c to a_1),

$$lA_l r_0^{l-1} = -\omega a_1 \sin(\omega t) \tag{58}$$

$$A_l = \frac{-\omega a_1}{k r_0^{kr_0}} \sin(\omega t). \tag{59}$$

We then have

$$\psi = \frac{-\omega a}{k r_0^{kr_0}} r^{kr_0} \sin(\omega t)\cos(kr_0\phi) \tag{60}$$

$$\frac{\partial \psi}{\partial r} = \frac{-\omega a}{r_0^{kr_0-1}} r^{kr_0-1} \sin(\omega t)\cos(kr_0\phi). \tag{61}$$

Substituting this result into eq 45 and eq 52, and constructing the Lagrangian as

$$L = \iint a^2 \left[\frac{1}{2}\rho \left(\frac{\omega^2}{k} \sin^2(\omega t) \cos^2(k r_0 \psi) \right) \right. \\ \left. - \frac{1}{2}\gamma \left(k^2 \cos^2(\omega t) \sin^2(k r_0 \phi) \right) \right] r_0^2 \cos\phi \, d\theta \, d\phi, \quad (62)$$

which, by integrating for the phase average as in the previous section, will return

$$\omega^2 = \frac{\gamma}{\rho} k^3, \quad (63)$$

identical to the dispersion relation for a flat surface.

That a constant surface curvature does not affect the dispersion of waves of a much smaller length should not come as a surprise. Aside from the great difference in length scale which we have imposed, the method used to find the dispersion relation concerns the derivatives of energy terms to obtain the dynamics of the system. The constant resting curvature cannot appear in such derivatives, and therefore should not have an effect on the linear system.

While we have considered a standing wave for analysis on the curved surface, the existence of travelling waves is not precluded. In the physical system we are primarily concerned with very small waves a long way from the boundary; dispersion and non-linear wave interaction act to prevent such very small waves forming a standing wave pattern.

References

(1) Faraday, M. On a Peculiar Class of Acoustical Figures; and on Certain Forms Assumed by Groups of Particles upon Vibrating Elastic Surfaces. *Philosophical Transactions of the Royal Society of London* **1831**, *121*, 299–340.

(2) Huang, N.; Shen, Z.; Long, S. A New View of Nonlinear Water Waves: The Hilbert Spectrum.

Annual Review of Fluid Mechanics **1999**, *31*, 417–457.

(3) Brunet, P.; Baudoin, M.; Matar, O.; Zoueshtiagh, F. Droplet displacements and oscillations induced by ultrasonic surface acoustic waves: A quantitative study. *Physical Review E* **2010**, *81*, 036315.

(4) Rezk, A.; Manor, O.; Friend, J. R.; Yeo, L. Y. Unique fingering instabilities and soliton-like wave propagation in thin acoustowetting films. *Nature Communications* **2012**, *3*.

(5) Alghane, M.; Chen, B. X.; Fu, Y. Q.; Li, Y.; Desmulliez, M. P. Y.; Mohammed, M. I.; Walton, A. J. Nonlinear hydrodynamic effects induced by Rayleigh surface acoustic wave in sessile droplets. *Phys. Rev. E* **2012**, *86*, 056304.

(6) Ohl, S.-W.; Ow, D. S.-W.; Klaseboer, E.; Wong, V. V.; Camattari, A.; Ohl, C.-D. Creation of cavitation activity in a microfluidic device through acoustically driven capillary waves. *Lab Chip* **2010**, *10*, 1848–1855.

(7) Xu, J.; Attinger, D. Control and ultrasonic actuation of a gas–liquid interface in a microfluidic chip. *Journal of Micromechanics and Microengineering* **2007**, *17*, 609.

(8) Tan, M. K.; Friend, J. R.; Matar, O. K.; Yeo, L. Y. Capillary wave motion excited by high frequency surface acoustic waves. *Physics of Fluids* **2010**, *22*, 112112.

(9) Shilton, R.; Yeo, L. Y.; Friend, J. Quantification of surface acoustic wave induced chaotic mixing-flows in microfluidic wells. *Sensors and Actuators B: Chemical* **2011**, *160*, 1565–1572.

(10) Li, H.; Friend, J.; Yeo, L. Surface acoustic wave concentration of particle and bioparticle suspensions. *Biomedical Microdevices* **2007**, *9*, 647–656.

(11) Kurosawa, M.; Watanabe, T.; Futami, A.; Higuchi, T. Surface acoustic wave atomizer. *Sensors and Actuators A: Physical* **1995**, *50*, 69–74.

(12) Qi, A.; Yeo, L.; Friend, J. Interfacial destabilization and atomization driven by surface acoustic waves. *Physics of Fluids* **2008**, *20*, 074103.

(13) Qi, A.; Yeo, L.; Friend, J.; Ho, J. The Extraction Of Liquid, Protein Molecules and Yeast Cells From Paper Through Surface Acoustic Wave Atomization. *Lab on a Chip* **2010**, *10*, 470–476.

(14) Heron, S. R.; Wilson, R.; Shaffer, S. A.; Goodlett, D. R.; Cooper, J. M. Surface acoustic wave nebulization of peptides as a microfluidic interface for mass spectrometry. *Analytical chemistry* **2010**, *82*, 3985–3989.

(15) Perlin, M.; Schultz, W. Capillary effects on surface waves. *Annual Review of Fluid Mechanics* **2000**, *32*, 241–274.

(16) Earnshaw, J.; Hughes, C. High-frequency capillary waves on the clean surface of water. *Langmuir* **1991**, *7*, 2419–2421.

(17) Friend, J. R.; Yeo, L. Y. Microscale Acoustofluidics: Microfluidics Driven via Acoustics and Ultrasonics. *Reviews of Modern Physics* **2011**, *83*, 647–704.

(18) Miyamoto, K.; Nagatomo, S.; Matsui, Y.; Shiokawa, S. Nonlinear vibration of liquid droplet by surface acoustic wave excitation. *Jpn. J. Appl. Phys* **2002**, *41*, 3465–3468.

(19) Falçon, E.; Laroche, C.; Fauve, S. Observation of gravity-capillary wave turbulence. *Physical Review Letters* **2007**, *98*, 94503.

(20) McGuiggan, P.; Grave, D.; Wallace, J.; Cheng, S.; Prosperetti, A.; Robbins, M. Dynamics of a Disturbed Sessile Drop Measured by Atomic Force Microscopy (AFM). *Langmuir* **2011**, *27*, 11966–11972.

(21) Vogel, V.; Moebius, D. Resonance of transverse capillary and longitudinal waves as a tool for monolayer investigations at the air-water interface. *Langmuir* **1989**, *5*, 129–133.

(22) Snouck, D.; Westra, M.-T.; van de Water, W. Turbulent parametric surface waves. *Physics of Fluids* **2009**, *21*, 025102.

(23) Kumar, S. Vibration-induced interfacial instabilities in viscoelastic fluids. *Physical Review E* **2002**, *65*, 026305.

(24) James, A.; Vukasinovic, B.; Smith, M.; Glezer, A. Vibration-induced drop atomization and bursting. *Journal of Fluid Mechanics* **2003**, *476*, 1–28.

(25) Barreras, F.; Amaveda, H.; Lozano, A. Transient high-frequency ultrasonic water atomization. *Experiments in Fluids* **2002**, *33*, 405–413.

(26) Douady, S. Experimental study of the Faraday instability. *Journal of Fluid Mechanics* **1990**, *221*, 383–409.

(27) Vukasinovic, B.; Smith, M.; Glezer, A. Dynamics of a sessile drop in forced vibration. *Journal of Fluid Mechanics* **2007**, *587*.

(28) Benjamin, T. B.; Ursell, F. The Stability of the Plane Free Surface of a Liquid in Vertical Periodic Motion. *Proceedings of the Royal Society of London A* **1954**, *225*, 505–515.

(29) Miles, J. W. Nonlinear Faraday Resonance. *Journal of Fluid Mechanics* **1984**, *146*, 285–302.

(30) Binks, D.; van de Water, W. Nonlinear Pattern Formation of Faraday Waves. *Physical Review Letters* **1997**, *78*, 4043–4046.

(31) Skeldon, A.; Porter, J. Scaling properties of weakly nonlinear coefficients in the Faraday problem. *Physical Review E* **2011**, *84*.

(32) Epstein, T.; Deegan, R. D. Strip waves in vibrated shear-thickening wormlike micellar solutions. *Physical Review E* **2010**, *81*, 1–7.

(33) Lang, R. Ultrasonic atomization of liquids. *The Journal of the Acoustical Society of America* **1962**, *34*, 6–8.

(34) Friend, J.; Yeo, L.; Arifin, D.; Mechler, A. Evaporative self-assembly assisted synthesis of polymeric nanoparticles by surface acoustic wave atomization. *Nanotechnology* **2008**, *19*, 145301.

(35) Xia, H.; Shats, M.; Punzmann, H. Modulation instability and capillary wave turbulence. *EPL (Europhysics Letters)* **2010**, *91*, 14002.

(36) Vega, J.; R udiger, S.; Viñals, J. Phenomenological model of weakly damped Faraday waves and the associated mean flow. *Physical Review E* **2004**, *70*, 046306.

(37) Newell, A. Wave Turbulence. *Annual Review of Fluid Mechanics* **2011**, *43*.

(38) Kolmogorov, A. The local structure of turbulence in incompressible viscous fluid for very large Reynolds numbers. *Proceedings of the Royal Society of London. Series A: Mathematical and Physical Sciences* **1991**, *434*, 9–13.

(39) Zakharov, V.; Dias, F.; Pushkarev, A. One-dimensional wave turbulence. *Physics Reports* **2004**, *398*, 1–65.

(40) Lee, W.; Kovačič, G.; Cai, D. Renormalized resonance quartets in dispersive wave turbulence. *Physical Review Letters* **2009**, *103*, 24502.

(41) Zakharov, V.; L'vov, V.; Falkovich, G. *Kolmogorov spectra of turbulence 1. Wave turbulence*; Springer, Berlin (Germany), 1992.

(42) Hansen, P.; Nicholson, D. Weak cubic Langmuir turbulence. *Physics of Fluids* **1983**, *26*, 3008.

(43) Falçon, E.; Fauve, S.; Laroche, C. Observation of intermittency in wave turbulence. *Physical Review Letters* **2007**, *98*, 154501.

(44) Extrand, C. W.; Moon, S. I. Contact Angles of Liquid Drops on Super Hydrophobic Surfaces: Understanding the Role of Flattening of Drops by Gravity. *Langmuir* **2010**, *26*, 17090–17099.

(45) Perez, M.; Brechet, Y.; Salvo, L.; Papoular, M.; Suery, M. Oscillation of liquid drops under gravity: Influence of shape on the resonance frequency. *Europhysics Letters* **1999**, *47*, 189–195.

(46) James, A.; Smith, M.; Glezer, A. Vibration-induced drop atomization and the numerical simulation of low-frequency single-droplet ejection. *Journal of Fluid Mechanics* **2003**, *476*, 29–62.

(47) Bechhoefer, J.; Ego, V.; Manneville, S.; Johnson, B. An experimental study of the onset of parametrically pumped surface waves in viscous fluids. *Journal of Fluid Mechanics* **1995**, *288*, 325–350.

(48) Tan, M.; Friend, J.; Yeo, L. Microparticle collection and concentration via a miniature surface acoustic wave device. *Lab Chip* **2007**, *7*, 618–625.

(49) Friend, J.; Yeo, L. Using laser Doppler vibrometry to measure capillary surface waves on fluid-fluid interfaces. *Biomicrofluidics* **2010**, *4*, 026501.

(50) Bell, J.; Rothberg, S. Laser vibrometers and contacting transducers, target rotation and six degree-of-freedom vibration: what do we really measure? *Journal of Sound and Vibration* **2000**, *237*, 245–261.

(51) Pushkarev, A.; Zakharov, V. Turbulence of capillary waves–theory and numerical simulation. *Physica D: Nonlinear Phenomena* **2000**, *135*, 98–116.

(52) Kartashova, E. Model of laminated wave turbulence. *JETP letters* **2006**, *83*, 283–287.

(53) Bostwick, J.; Steen, P. Capillary oscillations of a constrained liquid drop. *Physics of Fluids* **2009**, *21*, 032108.

(54) McHale, G.; Elliott, S.; Newton, M.; Herbertson, D.; Esmer, K. Levitation-free vibrated droplets: resonant oscillations of liquid marbles. *Langmuir* **2008**, *25*, 529–533.

(55) Lauterborn, W.; Cramer, E. Subharmonic route to chaos observed in acoustics. *Physical Review Letters* **1981**, *47*, 1445–1448.

(56) Thompson, C.; Mulpur, A.; Mehta, V.; Chandra, K. Transition to chaos in acoustically driven flows. *The Journal of the Acoustical Society of America* **1991**, *90*, 2097–2108.

(57) Moody, L. Friction factors for pipe flow. *Trans. Asme* **1944**, *66*, 671–684.

(58) Lighthill, S. Acoustic streaming. *Journal of Sound and Vibration* **1978**, *61*, 391–418.

(59) Tan, M. K.; Friend, J.; Yeo, L. Y. Interfacial jetting phenomena induced by focused surface vibrations. *Physical Review Letters* **2009**, *103*.

(60) Drazin, P. G. *Introduction to Hydrodynamic Stability*; Cambridge University Press, 2002.

(61) Longuet-Higgins, M. S. Mass transport in water waves. *Philosophical Transactions of the Royal Society of London. Series A, Mathematical and Physical Sciences* **1953**, *245*, 535–581.

(62) Trinh, E.; Wang, T. G. Large-amplitude free and driven drop-shape oscillations: experimental observations. *Journal of Fluid Mechanics* **1982**, *122*, 315–338.

(63) Mettu, S.; Chaudhury, M. K. Vibration Spectroscopy of a Sessile Drop and Its Contact Line. *Langmuir* **2012**, *28*, 14100–14106.

(64) Zakharov, V.; Filonenko, N. Weak turbulence of capillary waves. *Journal of Applied Mechanics and Technical Physics* **1967**, *8*, 37–40.

(65) Whitham, G. *Linear and nonlinear waves*; John Wiley & Sons, 1974.

This material is available free of charge via the Internet at `http://pubs.acs.org/`.